

PERFORMANCE AND DESIGN OF COMMERCIAL OFF-THE-SHELF (COTS) COMPONENTS-BASED MAGNETOMETER FOR FORESAIL-1 CUBESAT

Ville Lundén⁽¹⁾, Tatu Peltola⁽¹⁾, Petri Niemelä⁽¹⁾, Kiril Cheremetiev⁽¹⁾, Clayhills Bruce⁽¹⁾,
Minna Palmroth⁽²⁾, Emilia Kilpua⁽²⁾, Rami Vainio⁽³⁾, Pekka Janhunen⁽⁴⁾, Jaan Praks⁽¹⁾

⁽¹⁾ *Aalto University, Espoo, Finland*

⁽²⁾ *University of Helsinki, Helsinki, Finland*

⁽³⁾ *University of Turku, Turku, Finland*

⁽⁴⁾ *Finnish Meteorological Institute, Helsinki, Finland*

ABSTRACT

Magnetometers are among the most typical payloads on satellite missions. As the size and cost of satellites decrease and interest in CubeSats continually grows, the requirements for magnetometers continue evolving. Small size and low power consumption must be combined with low cost while achieving performance satisfying the stringent demands set by modern science missions. These requirements have inspired the development of the MAGnetometer Technology Test Instrument (MATTI). Developed by Aalto University, the novel magnetometer will fly as a secondary payload on-board the Foresail-1 CubeSat, a mission developed by the Finnish Centre of Excellence in Research of Sustainable Space (FORESAIL) and funded by the Academy of Finland.

Instead of having strictly defined science objectives, the primary objective of MATTI is to demonstrate what performance can be achieved by a design based completely on commercial off-the-shelf (COTS) components. In addition, MATTI will serve as a learning platform for future missions, like Foresail-2, with more stringent requirements set for magnetic experiments. This paper will present the design of MATTI along with results of the calibration and characterization campaigns performed to evaluate the performance of the instrument before the soon upcoming launch of Foresail-1 projected for early June 2022. The results show that MATTI achieves a noise level less than $1 \text{ nT}/\sqrt{\text{Hz}}$ at frequencies from 0.01 Hz to 15 Hz, and the measurement range of the instrument is $\pm 140 \mu\text{T}$.

1 INTRODUCTION

The development of high-performance anisotropic magneto-resistance (AMR) based magnetometers has been a topic of interest during the last few decades. In recent years, AMR magnetometers have reached levels of performance that can make them potential competitors for the more traditionally favored fluxgate magnetometers. AMR magnetometers still lag behind fluxgates in sensitivity [1, 2], but have the advantage especially in applications with strictly limited mass, volume, power, and financial budgets [3–5]. This makes state-of-the-art AMR magnetometers potentially attractive options for CubeSat science missions.

AMR sensors are typically widely available as low-cost (COTS) components [6]. Developing an AMR magnetometer fully based on easily available COTS components helps to reduce the costs and time used for the development of the instrument. However, COTS components can be a high-risk choice for space applications, as they are rarely radiation hardened and typically have no flight heritage. The MAGnetometer Technology Test Instrument (MATTI) is designed to act as a performance demonstration of a completely COTS components based AMR magnetometer for space applications.

The instrument is designed by Aalto University, and it will fly as a secondary payload on-board the Foreail-1 CubeSat.

2 DESIGN

The design of MATTI is built around three orthogonal AMR sensors from Honeywell. The HMC1001 and HMC1002 chips are used to achieve a triaxial configuration. The LT6234 differential operational amplifiers from Analog Devices are used to amplify sensor output before inputting it to the 24-bit multi-channel analog-to-digital converter from Texas Instruments, ADS131E08S. The data acquisition of MATTI is controlled by the STM32L431-series microcontroller unit (MCU). The MCU is also responsible for digital signal processing. All components of MATTI have been chosen with the goal of low power consumption in mind. Figure 1 shows an image of the flight model. Figure 2 presents the block diagram of MATTI showing its general structure.

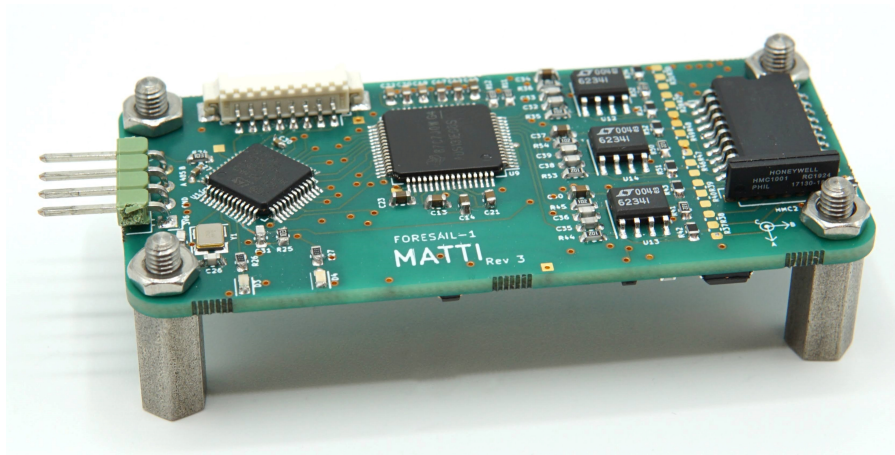


Figure 1: Flight model of MATTI. The dimensions of the instrument are 30 mm × 65 mm × 8 mm. Image courtesy of Aalto University.

In the absence of an ambient magnetic field, AMR sensors have a magnetization vector in the direction of their so called "easy axis". The direction perpendicular to the easy axis is known as the "sensitive axis". The resistance of the easy axis changes as a function of the magnetic field along the sensitive axis. Strong magnetic fields may corrupt the magnetization direction, and thus the performance of the sensor. [7] To avoid this, and to achieve high performance, MATTI implements a "flipping" or "set/reset pulsing" method typical for AMR magnetometers in high-performance applications [3, 8–11].

Set and reset pulses are short, high-current pulses with alternating polarity, driven through the sensors using dedicated set/reset straps integrated to the sensor chips. The set/reset pulses generate magnetic fields that restore and periodically flip the magnetization direction of the sensors. [12] To achieve high enough current pulse amplitudes, the supply voltage of MATTI is boosted. The approach leads to significantly improved performance, as parameters such as linearity, hysteresis, and noise [13], as well as offset [5] and cross-field effect cancellation [14], are improved.

3 TEST CAMPAIGN

3.1 Calibration

For the calibration of MATTI, a method developed by Riwanto *et al.* [15, 16] was used. The method

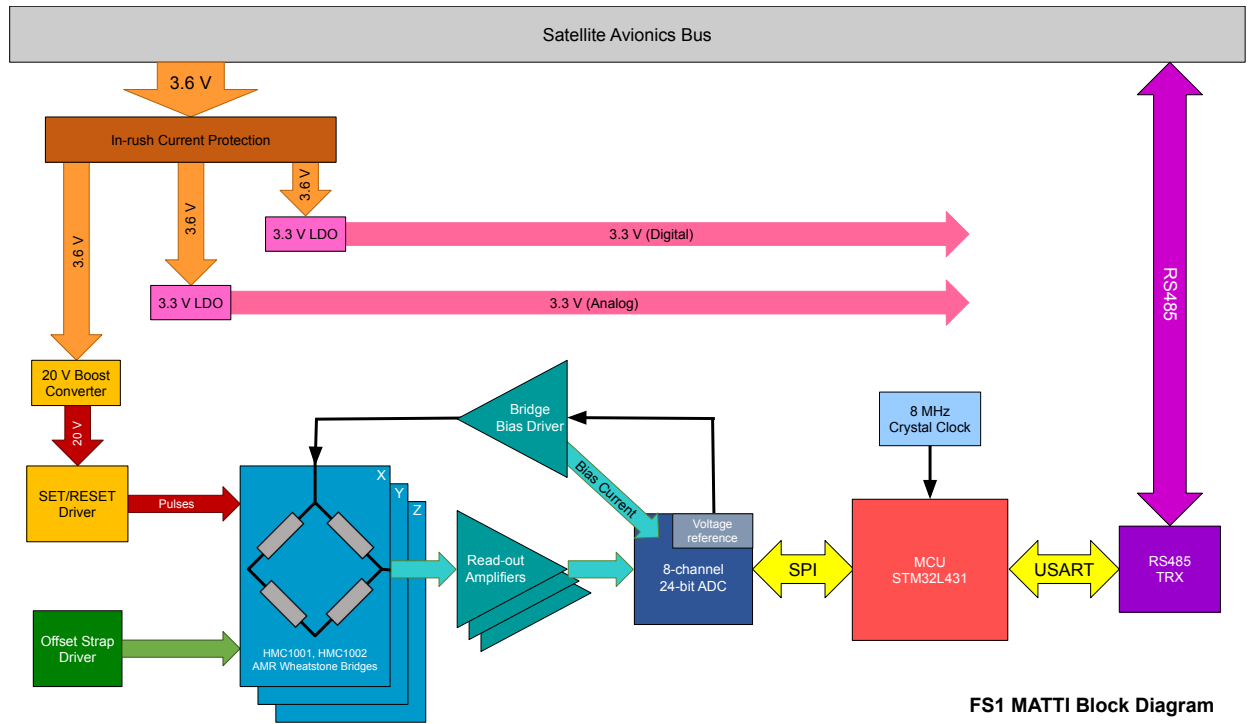


Figure 2: Block diagram of MATTI. The design choices of MATTI are illustrated by the diagram.

was chosen as it has been recently developed at Aalto University, designed for the equipment available, and the reported results [17] have proven it capable of satisfying the requirements set for the calibration and characterization of MATTI.

The detailed error model used as a basis for the calibration approach is derived by Riwanto *et al.* in [15], where they find the equation

$$\mathbf{b}_{\text{measured}} = \mathbf{S}_m \mathbf{N}_m^{-1} (1 + \mathbf{C}_{\text{si}}) (\mathbf{b}_{\text{ref}} + \mathbf{b}_{\text{hi}} + \mathbf{b}_{\text{off}} + \eta_m) \quad (1)$$

relating the actual ambient magnetic field \mathbf{b}_{ref} to the measurement results of the magnetometer, $\mathbf{b}_{\text{measured}}$. In the equation, \mathbf{S}_m is a 3×3 scale factor matrix, \mathbf{N}_m is a 3×3 matrix accounting for the non-orthogonalities of the sensors and \mathbf{C}_{si} is a 3×3 soft-iron parameter matrix. Additionally, the 3×1 vectors \mathbf{b}_{hi} and \mathbf{b}_{off} represent the hard-iron effects and the sensor offsets respectively, both manifesting as constant biases. Finally, the 3×1 vector η_m models the noise affecting the measurements. However, some of the error sources cannot be determined individually in practice. By combining these error sources, Riwanto *et al.* defined a simplified mathematical model of the sensors used for calibration by the equation

$$\mathbf{b}_{\text{measured}} = \mathbf{S}_m (\mathbf{b}_{\text{ref}} + \mathbf{b}_{\text{bias}} + \eta_m), \quad (2)$$

where $\mathbf{b}_{\text{measured}}$ is the measurement results of MATTI, \mathbf{S}_m is a 3×3 matrix combining the effects of individual error sources, \mathbf{b}_{ref} is the reference calibration field, \mathbf{b}_{bias} contains the total bias of the magnetometer, and η_m represents the effects of noise sources. From Eq. 2, the corrected magnetic field value $\mathbf{b}_{\text{corrected}}$ can be solved to be

$$\mathbf{b}_{\text{corrected}} = \mathbf{K}_m \mathbf{b}_{\text{measured}} - \mathbf{k}_m, \quad (3)$$

when assuming η_m to be zero-mean Gaussian random noise. Furthermore, $\mathbf{K}_m = \mathbf{S}_m^{-1}$, and $\mathbf{k}_m = \mathbf{b}_{\text{bias}}$. [15]

The method used to calculate the calibration parameters is based on a particle swarm optimization (PSO) algorithm by Riwanto *et al.* [15, 16]. The algorithm combines a scalar checking objective with a rotation axis fitting objective to obtain unambiguous calibration parameters. The algorithm assumes that a set of calibration data has been collected while the magnetic field around the magnetometer has been rotating around a static axis.

To achieve better calibration results, multiple different data sets with different rotation axes can be used for the calibration. Aiming to achieve optimal calibration performance, a Helmholtz coil system shown in Figure 3 was used to generate the fields required. The software controllable coil system can be used to generate nearly arbitrary static or dynamic magnetic fields inside the coils. The amplitude for the calibration was chosen to be 30 μT to roughly correspond to the expected magnetic field amplitude in orbit.



Figure 3: Helmholtz coil system used to calibrate MATTI. The three-axis coil system is located in a laboratory environment and surrounded by other electronics causing magnetic interference, especially at the mains frequency of 50 Hz. The black object in the middle of the coils is the reference fluxgate magnetometer used for calibration and characterization. Image courtesy of Aalto University.

The coils were driven to generate three separate loci of measurement points. A reference fluxgate magnetometer was used to verify the amplitude of the calibration field. The rotation axes of the loci were orthogonal. Using the data, the PSO algorithm calculated the calibration parameters for MATTI. The measurement loci are visualized in Figure 4. The loci are plotted both before and after calibration, which illustrates how calibrating the data fits the measurement loci on the sphere representing the reference field magnitude.

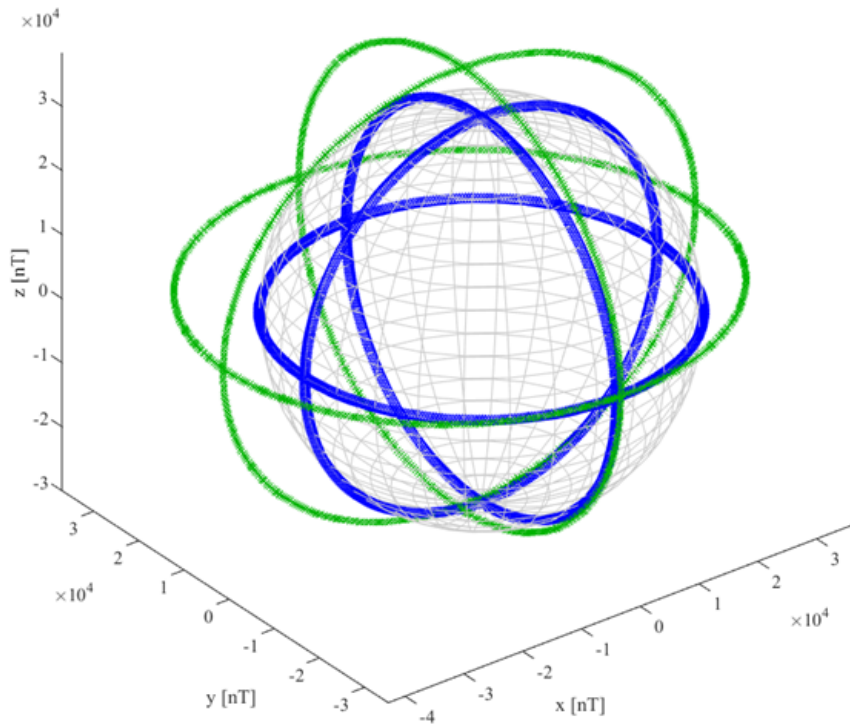


Figure 4: PSO calibration algorithm results. The figure is generated by a script part of the thesis work of Riwanto [17]. The axes present the field magnitude in units of nT. The green loci correspond to uncalibrated measurement data from MATTI, whereas the blue loci correspond to the same data after calibration. It can be seen that after calibration the data fits on the grey sphere representing the magnitude of the field used for calibration, 30 μ T.

The calibration was performed in a magnetically noisy laboratory environment. The amplitude of the calibration field is, however, over one magnitude higher than the amplitude of the noise, making it possible for the PSO algorithm to generate reliable and consistent calibration parameters. Consistency was confirmed by comparing the results of multiple calibration runs. The final calibration matrix \mathbf{K}_m and bias vector \mathbf{k}_m from Eq. 3 solved for the flight model of MATTI were shown to be

$$\mathbf{K}_m = \begin{bmatrix} 0.752742540954971 & -0.004704150388467 & -0.016786900331504 \\ 0.009779959234839 & 0.831869316066046 & -0.010914773404805 \\ 0.018806415207511 & -0.012757380140100 & 0.886138569910528 \end{bmatrix} \quad (4)$$

and

$$\mathbf{k}_m = \begin{bmatrix} 2426.339629917774 \\ 549.9438079800767 \\ 3817.173087134422 \end{bmatrix}. \quad (5)$$

The parameters from Eq. 4 and Eq. 5 scale the data of MATTI to units of nT.

3.2 Characterization

The available Helmholtz coil system was used for the characterization of MATTI. The linearity, offset, and gain of each axis of MATTI were determined by measuring static fields generated by the Helmholtz coils in the range of $\pm 200 \mu\text{T}$. A reference fluxgate magnetometer was used in the range of $\pm 100 \mu\text{T}$ to improve accuracy. Figure 5 shows how the output of MATTI depends on the ambient magnetic field. The linear response of the axis of MATTI depicted extends to roughly $\pm 140 \mu\text{T}$. Figure 6 shows a closer look at the linear region of the axis and the linear fit to the data. Other axes of MATTI behave essentially in the same way, and linearity parameters for all axes are shown in Table 1.

Table 1: Key linearity parameters of MATTI flight model.

Axis	Linear correlation ($\pm 100 \mu\text{T}$)	Gain ($\pm 100 \mu\text{T}$)	Linear range min/max (μT)
X	0.999997	1.0213	-140/150
Y	0.999996	1.0136	-140/150
Z	0.999997	1.0266	-140/190

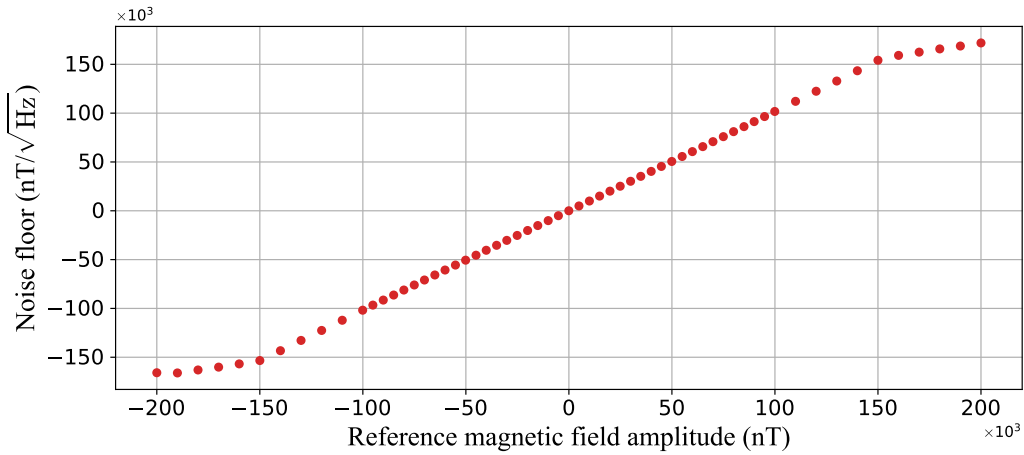


Figure 5: The response of an axis of MATTI to static fields in the range of $\pm 200 \mu\text{T}$. The vertical axis represents the measurement results of MATTI in units of nT. The horizontal axis displays the reference field amplitude applied in the same units. The graph shows that the linear region of MATTI is about $\pm 140 \mu\text{T}$ for the axis in question.

To determine the frequency response of MATTI, a magnetic field sweep over the bandwidth of 0.01 Hz to 20 Hz was generated using the Helmholtz coils. A fluxgate magnetometer was, again, used as a reference. The frequency attenuation of MATTI was determined by comparing its output amplitude to the reference. Figure 7 illustrates the frequency response of an axis of MATTI. Other axes have a virtually identical response, as can be observed from Table 2.

To characterize the noise floor limiting the sensitivity of MATTI, the instrument was placed inside a three-layer μ -metal chamber (Figure 8) that attenuates the ambient noise level. Continuous measurements lasted over 60 hours to ensure satisfactory frequency resolution at frequencies down to 0.01 Hz.

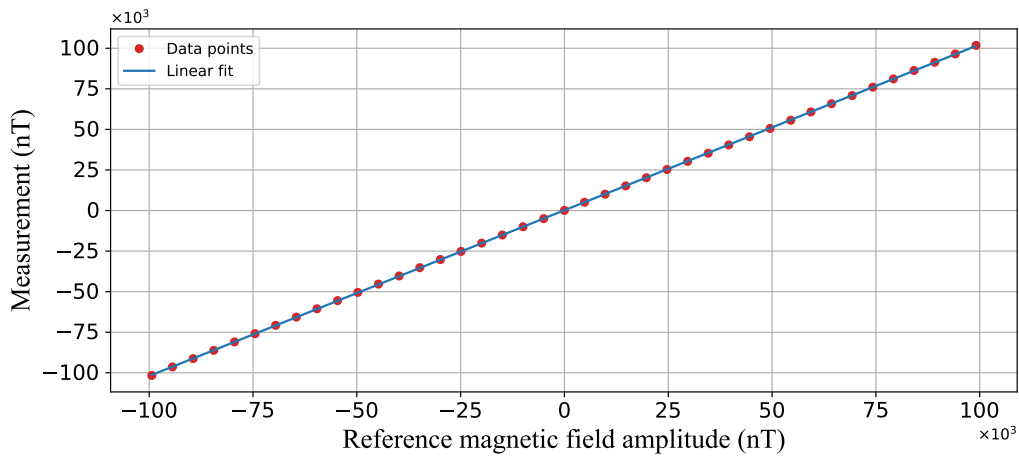


Figure 6: A linear fit to the seemingly linear region of MATTI from Figure 5 in the range of $\pm 100 \mu\text{T}$. The measurement results of MATTI and the reference field amplitude are presented by the vertical and horizontal axes of the graph respectively in units of nT. A linear fit estimation was calculated by using the least-squares method. Thus, the quality of linearity and the offsets of MATTI can be estimated. Estimated linearity parameters for the flight model of MATTI are specified in Table 1.

Table 2: Cutoff frequencies of the axes of MATTI flight model at different data rates.

Axis	Data rate 30 Hz	Data rate 10 Hz	Data rate 3 Hz
X	9.9 Hz	3.8 Hz	0.97 Hz
Y	9.9 Hz	3.8 Hz	0.97 Hz
Z	9.9 Hz	3.8 Hz	0.97 Hz

To obtain the noise floor, the amplitude spectral densities of the measurements were calculated. Results are illustrated in Figure 9 and summarized for certain frequencies in Table 3.

Table 3: Noise level of MATTI at certain frequencies.

Axis	Noise level @ 0.01 Hz ($\text{nT}/\sqrt{\text{Hz}}$)	Noise level @ 1 Hz ($\text{nT}/\sqrt{\text{Hz}}$)
X	0.39	0.37
Y	0.88	0.91
Z	0.49	0.44

The temperature dependence of MATTI was determined in two steps. A magnetically noisy thermal chamber was used to first calibrate the temperature sensor of MATTI. The temperature sensor could then be used to track the temperature of the instrument. Next, MATTI was warmed up, after which it started measuring while passively cooling down. Thus, the required magnetic field measurements

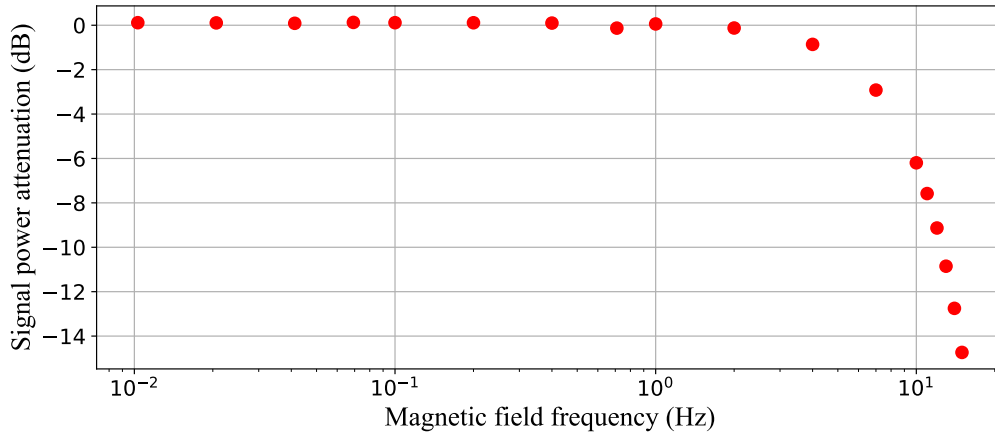


Figure 7: Frequency response of MATTI. The graph illustrates the frequency response of an axis of MATTI. The power attenuation of the signal of MATTI, presented in decibels on the vertical axis, is a function of the reference field frequency shown on the horizontal axis in units of Hz. The data was collected by measuring the magnetic field over a frequency sweep of 0.01 Hz to 20 Hz with MATTI and a reference magnetometer that undergoes no attenuation in the frequency range of interest. The sample rate of MATTI was 30 Hz and the cutoff frequency is shown to lie at 10 Hz. This is below the Nyquist frequency as required for adequate anti-aliasing.

were possible to perform during changing temperature of MATTI, under the influence of only the typical ambient noise level of the laboratory.

The temperature dependence was shown to be linear. The measurement data for one axis are depicted in Figure 10. The excessive laboratory noise present in the magnetometer signal was filtered out after the measurement, as otherwise the high noise level would corrupt the linear fit estimation. Table 4 presents the parameters solved for all axes. The temperature of MATTI during calibration, 26 °C, is used as the zero-drift reference temperature. Due to the lack of active, low-noise, cooling measures, the magnetometer was not cooled down below the temperature of the running instrument in ambient laboratory conditions.

Table 4: Temperature dependence parameters of each axis of MATTI.

Axis	Linear correlation	Temperature coefficient (nT/°C)
X	-0.968 168	-10.2
Y	0.975 793	5.43
Z	-0.973 595	-10.3

The absolute error of MATTI was not estimated due to the lack of a magnetically clean enough environment that could also incorporate a reference magnetometer. The estimation of the repeatability of MATTI was evaluated based on successive noise measurements performed in the μ -metal chamber, as it was the only environment capable of providing constant enough measurement conditions in terms of field and temperature stability. The repeatability was quantified using standard deviation, and results are presented in Table 5.

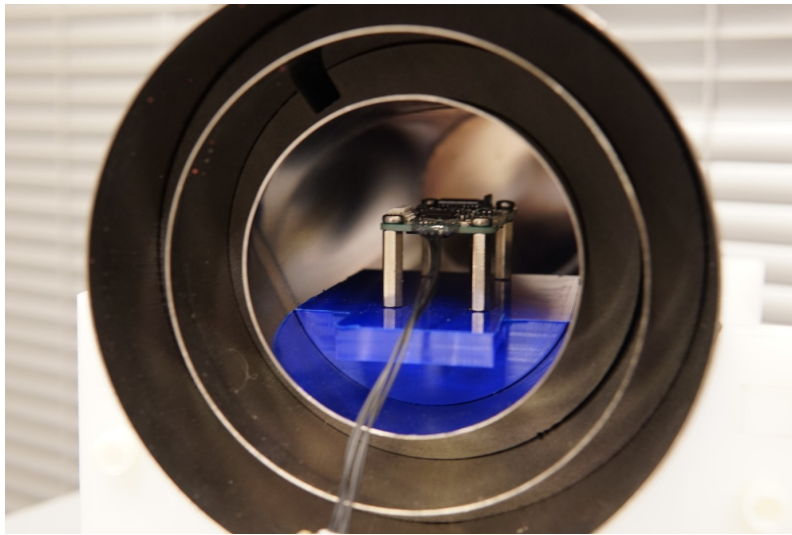


Figure 8: MATTI inside a three-layer μ -metal chamber. The chamber attenuates the ambient magnetic field by a factor off approximately 1500 [18]. Image courtesy of Aalto University.

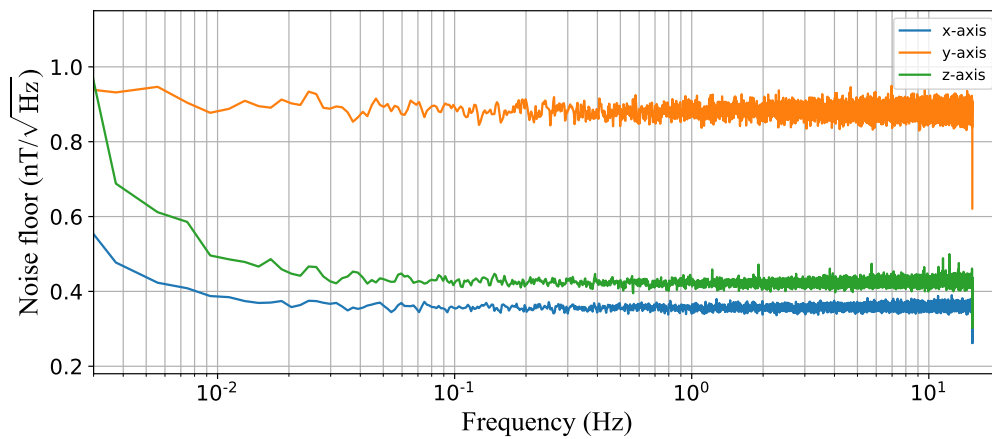


Figure 9: The noise floor of each axis of MATTI. The vertical axis shows the noise floor in $\text{nT}/\sqrt{\text{Hz}}$, whereas the horizontal axis represents the frequency of the noise in units of Hz.

Table 5: Repeatability parameters of MATTI. The standard deviation of consecutive measurements in constant conditions is used as the measure of repeatability.

Axis	Standard deviation (nT)
X	1.88
Y	3.70
Z	2.44

Finally, the power consumption of MATTI was determined by a power analyzer. The average power consumption of the instrument was shown to be 0.18 W.

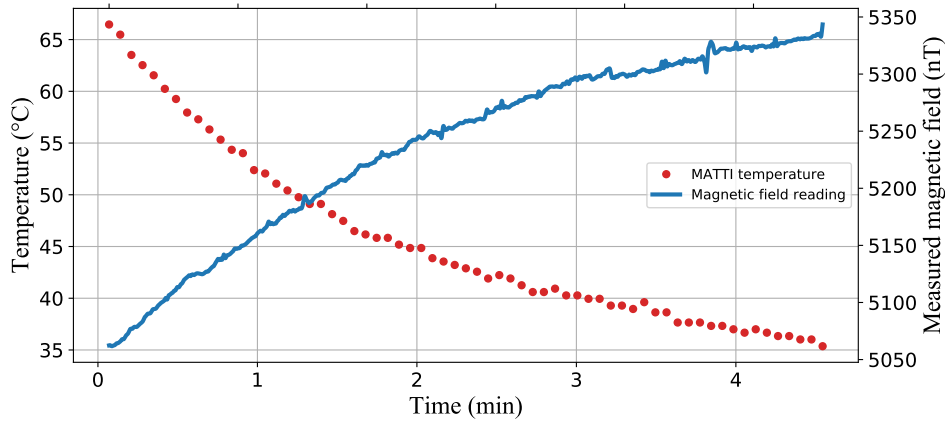


Figure 10: Temperature dependency of an axis of MATTI. The response of only one axis is plotted for illustrative reasons. The temperature of MATTI is presented on the left vertical axis in units of °C, whereas the amplitude of the magnetic field measurements of the axis are exhibited on the right in nT. The common horizontal axis presents the time since the start of the measurement in minutes. The temperature dependency of the axis is shown to be linear with a correlation coefficient of -0.97 equaling a strong linear correlation. The negative temperature coefficient for the axis is determined to be -10.2 nT/°C.

4 CONCLUSIONS

In this paper, the design, calibration, and characterization of a novel high-performance AMR magnetometer, MATTI, was presented. The calibration campaign was successfully implemented in a typical laboratory environment, further confirming the suitability of the chosen calibration method for high-performance magnetometer calibration in noisy conditions. The high ambient noise level of the laboratory did not affect the calibration results.

For the characterization process, however, the main challenges were associated with the high noise level of the laboratory and some equipment used. Some characteristics, like the temperature dependence, were determined by methods that were modified to avoid using equipment that could corrupt the measurement results by disturbing the magnetic field. Consequently, the temperature was not cooled down below room temperature. Hence, the trade off of the approach was, that the temperature dependence could not be explicitly determined for the whole range of temperatures where MATTI is expected to operate. In the future, this could, for instance, be achieved by cooling down the instrument in a thermally insulated container filled with a suitable cooling agent lowering the temperature of MATTI.

Another factor potentially further enhancing the quality of characterization results could be increased averaging. By averaging characterization results over multiple separate characterization runs, especially the effects of noise can be better mitigated. This could directly improve the reliability of the magnetometer's characteristic parameters. Averaging could be used to improve calibration results as well.

To conclude, the achieved characterization performance is sufficient to fulfill the requirements set for the characterization of MATTI. Additionally, the characterization confirms that the calibration of the instrument was successful, and most importantly, the characterization shows that MATTI achieves the performance requirements set for it. MATTI reaches a noise level less than 1 nT/ $\sqrt{\text{Hz}}$ at frequencies from 0.01 Hz to 15 Hz, with a measurement range of ± 140 μT .

References

- [1] A. L. Herrera-May, L. A. Aguilera-Cortés, P. J. García-Ramírez, and E. Manjarrez, “Resonant magnetic field sensors based on mems technology,” *Sensors*, vol. 9, no. 10, pp. 7785–7813, 2009. DOI: [10.3390/s91007785](https://doi.org/10.3390/s91007785).
- [2] D. Novotný, V. Petrucha, and M. Janošek, “A digitally compensated amr magnetometer,” *IEEE Trans. Magn.*, vol. 55, no. 1, pp. 1–5, 2019. DOI: [10.1109/TMAG.2018.2873235](https://doi.org/10.1109/TMAG.2018.2873235).
- [3] P. Brown *et al.*, “Magnetoresistive magnetometer for space science applications,” *Meas. Sci. Technol.*, vol. 23, no. 2, p. 025 902, 2012. DOI: [10.1088/0957-0233/23/2/025902](https://doi.org/10.1088/0957-0233/23/2/025902).
- [4] S. Singh *et al.*, “Analysis and comparison of calibration techniques for cots sensors onboard a nanosatellite,” in *2019 IEEE Aerospace Conference*, 2019, pp. 1–11. DOI: [10.1109/AERO.2019.8742132](https://doi.org/10.1109/AERO.2019.8742132).
- [5] D. Novotny, V. Petrucha, M. Dressler, and A. Platil, “Characterization of a digital amr magnetometer for space applications,” *IEEE Trans. Instrum. Meas*, vol. 70, pp. 1–9, 2021. DOI: [10.1109/TIM.2020.3043867](https://doi.org/10.1109/TIM.2020.3043867).
- [6] L. Schulz, P. Heinisch, and I. Richter, “Calibration of off-the-shelf anisotropic magnetoresistance magnetometers,” *Sensors*, vol. 19, no. 8, 2019. DOI: [10.3390/s19081850](https://doi.org/10.3390/s19081850).
- [7] K. Mohamadabadi, “Anisotropic magnetoresistance magnetometer for inertial navigation systems,” English, Doctoral thesis, Ecole Polytechnique X, Nov. 2013, 130 pp. [Online]. Available: <https://tel.archives-ouvertes.fr/tel-00946970/>.
- [8] F. Qiu, J. Wang, Y. Zhang, G. Yang, and C. Weng, “Resolution limit of anisotropic magnetoresistance(amr) based vector magnetometer,” *Sens. Actuator. A Phys.*, vol. 280, pp. 61–67, 2018. DOI: [10.1016/j.sna.2018.07.031](https://doi.org/10.1016/j.sna.2018.07.031).
- [9] P. Ripka, M. Vopálenský, A. Platil, M. Döscher, K.-M. Lenssen, and H. Hauser, “Amr magnetometer,” *J. Magn. Magn. Mater.*, vol. 254-255, pp. 639–641, 2003. DOI: [10.1016/S0304-8853\(02\)00927-7](https://doi.org/10.1016/S0304-8853(02)00927-7).
- [10] N. Hadjigeorgiou, K. Papafotis, and P. P. Sotiriadis, “Exploring amr sensors’ performance limits using an agile, high-speed set–reset pulse generation circuit,” *IEEE Trans. Magn.*, vol. 56, no. 9, pp. 1–10, 2020. DOI: [10.1109/TMAG.2020.3009870](https://doi.org/10.1109/TMAG.2020.3009870).
- [11] P. Brown *et al.*, “Space magnetometer based on an anisotropic magnetoresistive hybrid sensor,” *Rev. Sci. Instrum.*, vol. 85, no. 12, p. 125 117, 2014. DOI: [10.1063/1.4904702](https://doi.org/10.1063/1.4904702).
- [12] N. Hadjigeorgiou, K. Asimakopoulos, K. Papafotis, and P. P. Sotiriadis, “Vector magnetic field sensors: Operating principles, calibration, and applications,” *IEEE Sens. J.*, vol. 21, no. 11, pp. 12 531–12 544, 2021. DOI: [10.1109/JSEN.2020.3045660](https://doi.org/10.1109/JSEN.2020.3045660).
- [13] I. Mateos, J. Ramos-Castro, and A. Lobo, “Low-frequency noise characterization of a magnetic field monitoring system using an anisotropic magnetoresistance,” *Sens. Actuator. A Phys.*, vol. 235, pp. 57–63, 2015. DOI: [10.1016/j.sna.2015.09.021](https://doi.org/10.1016/j.sna.2015.09.021).
- [14] P. Ripka, M. Janosek, and M. Butta, “Crossfield sensitivity in amr sensors,” *IEEE Trans. Magn.*, vol. 45, no. 10, pp. 4514–4517, 2009. DOI: [10.1109/TMAG.2009.2022051](https://doi.org/10.1109/TMAG.2009.2022051).
- [15] B. A. Riwanto, T. Tikka, A. Kestilä, and J. Praks, “Particle swarm optimization with rotation axis fitting for magnetometer calibration,” *IEEE Trans Aerosp Electron Syst*, vol. 53, no. 2, pp. 1009–1022, 2017. DOI: [10.1109/TAES.2017.2667458](https://doi.org/10.1109/TAES.2017.2667458).

- [16] B. A. Riwanto, P. Niemelä, H. Ehrpais, A. Slavinskis, M. R. Mughal, and J. Praks, “Particle swarm optimization for magnetometer calibration with rotation axis fitting using in-orbit data,” *IEEE Trans. Aerosp. Electron. Syst.*, 2021, Accepted for publication. DOI: [10.1109/TAES.2021.3122514](https://doi.org/10.1109/TAES.2021.3122514).
- [17] B. A. Riwanto, “Calibration and testing techniques for nanosatellite attitude system development in magnetic environment,” English, Doctoral thesis, School of Electrical Engineering, 2021, 72 pp., ISBN: 978-952-64-0460-8. [Online]. Available: <http://urn.fi/URN:ISBN:978-952-64-0460-8>.
- [18] Magnetic Shield Corp., “Catalog ZG-3: Zero Gauss Chambers,” Product catalog, 2013. [Online]. Available: <https://store-w4rbnih33r.mybigcommerce.com/content/ZG-3-brochure-web%281%29%281%29-REV-3-17-15.pdf>.